Q. J. R. Meteorol. Soc. (1994), **120**, pp. 79–109 551.558.21 (941)

Airflow over a two-dimensional escarpment. III: Nonhydrostatic flow

By J. A. BLOCKLEY and T. J. LYONS*
Murdoch University, Australia

(Received 3 August 1992; revised 30 June 1993)

SUMMARY

Forced flow over the asymmetric topography of the Darling Scarp, Western Australia is modelled, using a nonhydrostatic model, and compared with observations. Drag histories and sensitivity tests indicate that it is possible for the flow to be dominated by hydrostatic downslope windstorms even if the hydrostatic index indicates nonhydrostatic dominance. Experiments on a wide range of one- or two-layered flows suggest that nonhydrostatic effects on windstorm events are very small. However, the development and location of trapped lee waves can be significantly affected if there is sufficient hydrostatic forcing in the flow. For hydrostatic forcing to dominate over trapped lee waves it is necessary for reflection, from a region of wave breaking or a critical layer, to occur at the right height.

1. INTRODUCTION

The structure and type of wave excited by airflow over isolated obstacles can be differentiated in terms of the mountain half-width, a, Brunt–Väisälä frequency, N, and wind speed, U. Assuming N/U is independent of height and $Ua^{-1} \gg N$, the dominant wave numbers will be greater than N/U and the disturbance will decay exponentially with height as an evanescent wave. Alternatively, if $Ua^{-1} \ll N$, the dominant wave number will be less than N/U and the disturbance will propagate vertically with lines of constant phase tilting upstream. Smith (1979) noted that the vertical accelerations that permit waves to decay exponentially with height imply that evanescent waves are essentially a nonhydrostatic effect.

For bell-shaped hills, the maximum contribution to the energy spectrum occurs at $k = a^{-1}$, where k is the wave number (Klemp and Lilly 1980). Klemp and Lilly (1980) found from linear theory that maximum vertical energy propagation, and hence hydrostatic forcing, would occur for flow over a bell-shaped hill with $Na/U \sim 10$. As Na/U decreased from 10 the maximum angle of energy propagation approaches zero and the flow becomes increasingly nonhydrostatic.

Further differentiation of flow types is possible by examining changes in the vertical structure of wind speed and stability. Scorer (1949) showed that waves can be defined in terms of Scorer's parameter, l^2, given by

$$l^2 = \frac{N^2}{U^2} - U^{-1}\frac{\mathrm{d}^2 U}{\mathrm{d}z^2}$$

where z is height.

The Scorer parameter is very sensitive to the second derivative of the wind speed, which is difficult to measure accurately and is only significant in regions where there are strong variations in wind shear. Consequently most authors tend to neglect this term, approximating the Scorer parameter by N/U.

In atmospheres where l^2 decreases strongly aloft, wave energy is trapped in the lower layers, allowing the formation of a trapped lee wave. These waves are formed by the constructive interference between up-going and down-going waves in which the latter

* Corresponding author: School of Biological and Environmental Sciences, Murdoch University, Perth, WA6150, Australia.

exists because of a strong partial reflection of the nonhydrostatic component of the wavefield at some height above the ground (Smith 1979). As a result of the limit to the vertical propagation of energy, trapped lee waves may propagate for large distances downstream and frequently have been observed to the lee of mountains and hills.

The linear theory developed by Scorer (1949) for a two-layer atmosphere has been extended by others (e.g. Sawyer 1960; Vergeiner 1971; Simard and Peltier 1982) to more realistic temperature and wind-speed profiles using numerical techniques. Vergeiner (1971) and Mitchell *et al.* (1990), amongst others, have attempted to compare linear lee-wave theory with observed lee-wave amplitude and wavelength. Mitchell *et al* (1990) examined the formation of lee waves over Macquarie Island and obtained good agreement between linear theory and observed wavelength. Vergeiner (1971) obtained what appear to be good comparisons of both wavelength and amplitude.

However, Smith (1976) suggested that Vergeiner (1971) had to use unrealistically narrow topography in order to obtain similar amplitudes between model and observed lee waves. In his review of atmospheric flow over mountains, Smith (1979) noted that it was relatively easy to get good agreement between observed and predicted wavelengths as these never vary by more than a factor of two or three in the real atmosphere.

In contrast, lee-wave amplitudes are somewhat harder to model accurately as the linearized bottom boundary condition may reduce the effective mountain height (Peltier and Clark 1983). Smith (1976) compared model values with those of lee waves observed over the Blue Ridge, and obtained model values of amplitudes that were around a factor of four less than those observed. He suggested that hydrostatic forcing of lee waves may have forced the departure of the linear theory predicted lee-wave amplitude from that observed, as a result of the strong nonlinearity in the governing equations.

Variations in the vertical structure of the atmosphere also may have a significant role to play in the formation of wave structures forced by larger-wavelength waves. A critical layer occurs where the horizontal wind speed becomes zero at some point above the mountain. A number of authors (Clark and Peltier 1984; Durran and Klemp 1987; Bacmeister and Pierrehumbert 1988; Scinocca and Peltier 1991) have implicated reflection of vertically propagating gravity waves off the critical layer in the formation of strong downslope winds. Current debate has focused on the nature and phase of these reflections, being divided between the hydraulic-like theories discussed by Smith (1985), Durran (1986) and Bacmeister and Pierrehumbert (1988) and the resonantly over-reflected mode of shear instability originally suggested by Peltier and Clark (1979) and Clark and Peltier (1984) and more recently elucidated by Laprise and Peltier (1989).

Common to both theories is the importance of wave breaking, either caused by vertically propagating waves breaking against the critical layer (Bacmeister and Pierrehumbert 1988) or induced by topography. That is if the streamline of the gravity wave above the mountain becomes vertical then the flow in this region becomes convectively unstable and the wave breaks (Peltier and Clark 1979).

The previous discussion highlights different wave structures produced when the flow is dominated by either very high or very low wave numbers, and the modifying effect that vertical structure has upon these waves. However, within the real atmosphere there is a spectrum of wave numbers which raises the question as to how these different wave numbers interact. Scinocca and Peltier (1989) demonstrated that the nonhydrostatic trapped-lee-wave component is erased when the hydrostatic component breaks, leading to downstream expansion of the low-level jet and overlying mixed region, and to the Kelvin–Helmoltz instability of this sheared structure. In the case where there is still significant hydrostatic forcing, but where wave breaking does not occur, it is not well understood how the hydrostatic and nonhydrostatic components interact. It is the purpose

of this paper to investigate the development of nonhydrostatic topographically induced waves in a complex atmosphere.

The waves being studied are generated by airflow over the 300 m Darling Scarp near Perth, Western Australia. This escarpment marks the western edge of an extensive inland plateau that descends to the Swan coastal plain in 3–5 km while stretching for approximately 200 km in a north–south direction. Pitts and Lyons (1989) observed both hydrostatic and nonhydrostatic waves under strong synoptic easterly winds over the escarpment, and showed that the observed flow fields were essentially two dimensional. These flows were characterized by shallow easterly winds that turn westerly aloft. They suggested that the flow could be differentiated using an averaged hydrostatic index Na/U, within the lower layer, with values greater than 4.8 (approximately), leading to hydrostatically dominated flow (Pitts and Lyons 1990).

Two of the days, 13 December 1986 and 3 February 1987, when the flows were hydrostatically dominated, have been modelled by Pitts and Lyons (1990) using a hydrostatic mesoscale model. This successfully reproduced the general features of the flow, but did not incorporate nonhydrostatic features, such as lee waves or rotors. This paper seeks to extend those studies to the observed nonhydrostatic flows, using a nonhydrostatic numerical model and a linear lee-wave model, as well as to investigate the role of hydrostatic forcing on such days.

2. The models

(a) *Linear model*

While it is true that exact solutions for lee waves excited by flow over isolated mountains do exist these can only be formulated for a small number of idealized wind and temperature profiles. In order to examine arbitrarily specified profiles it is necessary to incorporate some numerical approximations (Sawyer 1960; Simard and Peltier 1982). Much work has been done to describe linear solutions of flow over hills (e.g. Scorer 1949; Sawyer 1960; Vergeiner 1971) and the model we have used follows the formulation of Mitchell *et al.* (1990) and Sawyer (1960).

Assuming two-dimensional flow and neglecting nonlinearities, the wave equation may be written (Sawyer 1960; Mitchell *et al.* 1990)

$$\frac{\mathrm{d}^2\psi}{\mathrm{d}z^2}(k, z) + \{l^2(z) - k^2\}\psi(k, z) = 0$$

where ψ is related to the stream function ϕ by the equations

$$\psi(k, z) = \left(\frac{\rho(z)}{\rho(0)}\right)^{\frac{1}{2}} \phi(k, z)$$

where ρ is the air density, and

$$\phi(x, z) = \int_0^\infty \mathrm{d}k\, \phi(k, z)\mathrm{e}^{ikx}.$$

By assuming appropriate boundary conditions and l^2 profile, lee waves are found as eigenvalues of the wave equation. Sawyer (1960) derived a full numerical solution for the streamline displacement, using contour integration and the theorem of residues. However, the approximate solution of Scorer (1949) is sufficient except in the immediate

vicinity of the ridge (Mitchell *et al.* 1990) and thus we have taken the streamline displacement as

$$\xi(x, z) = Re\left(\frac{\rho(0)}{\rho(z)}\right)^{\frac{1}{2}} \frac{U(0)}{U(z)} ha \left(\frac{f(0, z)}{f(0, 0)} \frac{(a + ix)}{(a^2 + x^2)} + 2\pi i \sum_m \frac{f(k_m, z)}{f'(k_m, 0)} \exp(-k_m a + ik_m x)\right)$$

for $x \geq 0$

and

$$\xi(x, z) = Re\left(\frac{\rho(0)}{\rho(z)}\right)^{\frac{1}{2}} \frac{U(0)}{U(z)} ha \frac{f(0, z)}{f(0, 0)} \frac{(a + ix)}{(a^2 + x^2)} \qquad \text{for } x < 0$$

where f is a function which satisfies the wave equation under boundary conditions of requiring the wave amplitude to be zero at the ground and decaying with increasing height (Mitchell *et al.* 1990), $f'(k_m, 0)$ the derivative of f with respect to wave number, Re the Reynolds number and h the ridge height.

The ridge shape does not in itself enter linear theory apart from providing a lower-boundary condition on the stream function. That is, the hill profile given by

$$H(x) = \frac{ha^2}{a^2 + x^2}$$

provides the contour for the streamline at $z = h(x)$.

Following Scorer (1949), the model was initialized with wind-speed and temperature profiles that ensured a constant l^2 in each layer. Wind speed was prescribed using

$$U(z) = \left(2.25 \tanh\left(\frac{2000 - z}{750}\right) + 14.5\right)$$

whereas the temperature profile was specified by dividing the atmosphere into three layers with constant N in each layer. That is

$$N = 0.016\ \text{s}^{-1} \qquad 0 < Z \leq 1200$$

$$N = 0.017\ \text{s}^{-1} \qquad 1200 < Z \leq 2640$$

$$N = 0.009\ \text{s}^{-1} \qquad 2640 < Z < 4800.$$

Figure 1 illustrates the linear-model solution for this atmosphere, yielding lee waves with wavelengths of 7.6 km and a maximum amplitude of 370 m.

(*b*) *Nonlinear model*

The nonlinear model is based on the Regional Atmospheric Modelling System (RAMS) developed by Tremback *et al.* (1985). This model can be configured either hydrostatically or nonhydrostatically. The nonhydrostatic version employs a fully compressible time-split model with a leap-frog advective scheme (Tripoli and Cotton 1982), whereas the hydrostatic version uses a 6th order time-split scheme with forward–backward finite differencing (Tremback *et al.* 1985). All other options were held constant between the two versions, and turbulence closure was achieved using local first-order eddy viscosity (Tripoli and Cotton 1982).

To minimize reflections at the lateral boundaries a pseudo-radiative boundary condition was employed (Orlanski 1976). Davies (1983) noted that significant errors may occur with radiative boundary schemes if phase perturbing effects, such as those caused by orography, are situated close to the boundaries. Furthermore Scinocca and Peltier

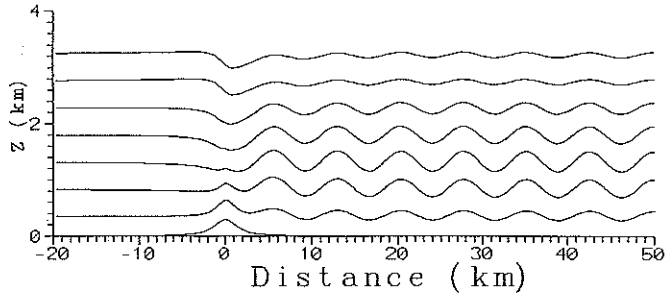

Figure 1. Linear-model solution for flow over a bell-shaped hill. Flow is from left to right.

(1989) observed that simulations carried out over long time-scales can be very sensitive to the horizontal extent of the model domain. Thus a horizontal domain of $150\Delta X$ was employed for the nonhydrostatic model. The hydrostatic version is less sensitive as a result of the reduced horizontal wave propagation and so a horizontal domain of $100\Delta X$ was employed for computational efficiency.

In the vertical the model used a stretched grid with the highest resolution being in the boundary layer with a ΔZ of 50 m. At the top of the model domain ΔZ was 200 m, and 68 grid points were used in the vertical domain. To minimize reflections from the upper boundary the Klemp and Durran (1983) radiative boundary condition was employed.

Aliasing of short-wavelength waves was controlled through the application of an explicit filter after Long (McNider and Pielke 1984), given as

$$(1-\beta)\Phi_{i+1}^{t+1} + 2(1+\beta)\Phi_i^{t+1} + (1-\beta)\phi_{i-1}^{t+1} = \phi_{i+1}^{t+1} + 2\phi_i^t + \phi_{i-1}^t$$

where ϕ_i^{t+1} is the filtered value at point i, ϕ_i^t is the original value, and β is the filter coefficient. A value of 0.007 for the filter coefficient was found to be sufficient to control numerical instabilities without over damping the relatively short-wavelength lee waves.

Previous investigations of forced flows over topography have shown that where the boundary-layer depth and hill length-scales are of a similar magnitude, the inclusion of the boundary layer is essential to reproduce observed flows (Richard *et al.* 1989; Pitts and Lyons 1990). Thus we prescribed a stable boundary layer with no surface heating, similar to that used by Pitts and Lyons (1990).

The average profile of the Darling Scarp is well represented by a half-bell-shaped hill of half width 1600 m and height 300 m. The largest horizontal resolution that is able to resolve this requires a ΔX of 533 m (Pitts and Lyons 1990) and hence the topography used in the simulations is described by

$$z(x) = \begin{cases} \dfrac{ha^2}{a^2 + x^2} & -75\Delta x < x \leqslant 0 \\ h & 0 < x \leqslant 75\Delta x \end{cases}.$$

Given the large number of options available in the model and the complex manner in which they could interact, the model configuration was validated against the analytical solution of Klemp and Durran (1983). These solutions are representative of Boussinesq hydrostatic flows, with constant wind and stability, over a two-dimensional bell-shaped mountain. As the flows are irrotational and inviscid, the boundary layer was turned off and the Coriolis forced neglected.

Figure 2(a) gives the model solution for a bell-shaped hill of height 300 m, half width 6000 m, wind speed 12 m s^{-1} and a Brunt–Väisälä frequency 0.02 s^{-1}. Simulations are for a non-dimensional time (Ut/a) of 60, at which the model had reached steady state. Klemp and Durran's (1983) solution (Fig. 2(b)) is similar, although ours is more damped, particularly in the upper layers. This results from filtering to control aliased waves and the application of an Asselin filter (Asselin 1972; Cotton and Tripoli 1978) to control the computational mode associated with leap-frog finite differencing.

Lee waves are typically of short wavelength, and the model's capacity to resolve these features was validated against the two-layer numerical solution of Durran (1986), in which the model was initialized with N as 0.025 and 0.01 s^{-1} in the lower and upper layers, respectively, and the wind speed was a constant 25 m s^{-1}. Figure 2(c) shows the simulation for non-dimensional time 25 compared with the simulation of Durran (1986) at non-dimensional time 20 (Fig. 2(d)). These are similar, although our solutions are more damped particularly near the downwind boundary. Our simulation was computed over a longer time to determine whether any difference between the two models was a result of our simulations not reaching a steady state after a non-dimensional time of 20. There was, however, little strengthening of the wave between time 20 and 25. The solutions were very sensitive to the application of Long's filter, as varying the filter coefficient between 0.007 and 0.05 completely removed lee waves.

Figure 2(e) illustrates the simulation for the linear case of Fig. 1. In this the calculated wavelength is 7.8 km and the maximum lee-wave amplitude 391 m, in comparison with the corresponding figures of 7.6 km and 370 m found in the linear solution. Unlike the linear solution these lee waves illustrate a slight damping as they move downstream.

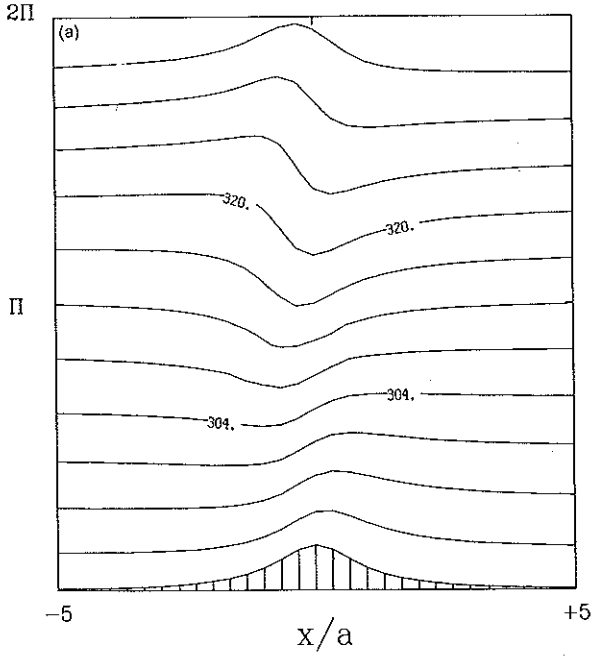

Figure 2. Model simulations of (a) isentropic surfaces for Klemp and Durran's (1983) analytical solution (b) for flow over a bell-shaped hill; (c) isentropic surfaces for Durran's (1986) numerical solution (d); and (e) isentropic surfaces for a two-layer atmosphere as modelled by the linear model. Flow is from left to right.

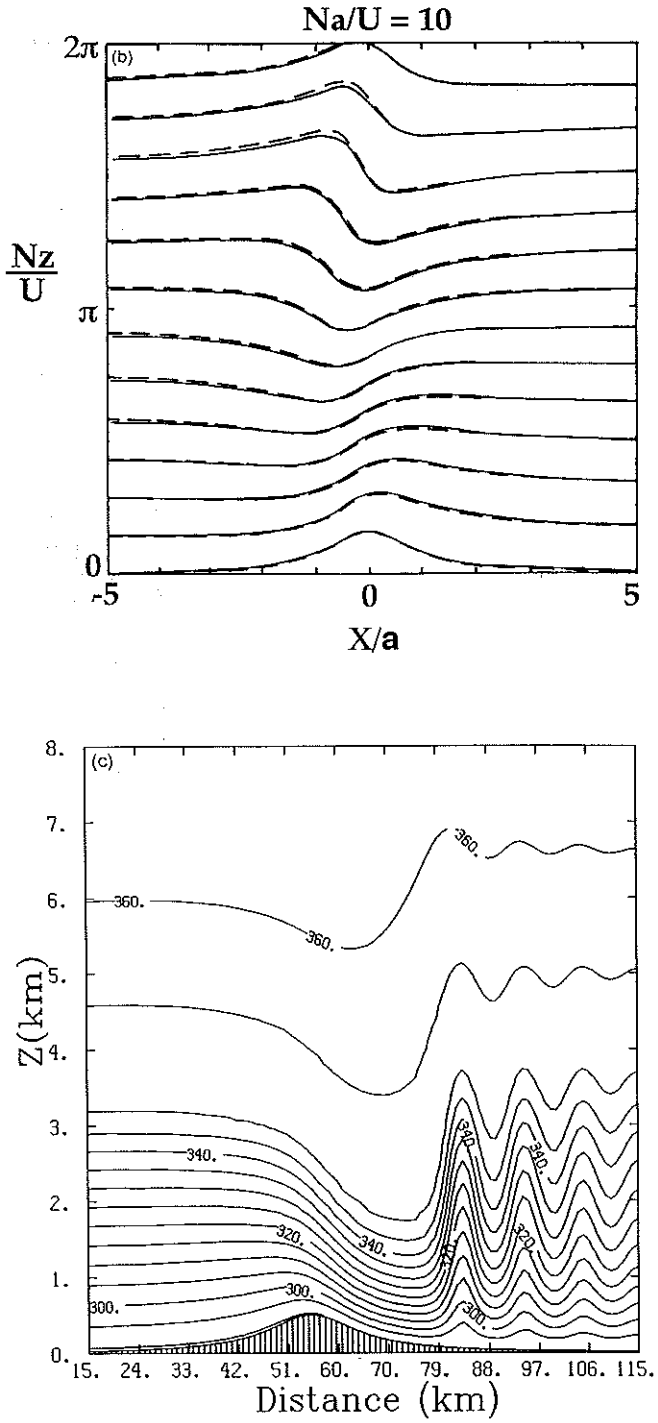

Figure 2. Continued.

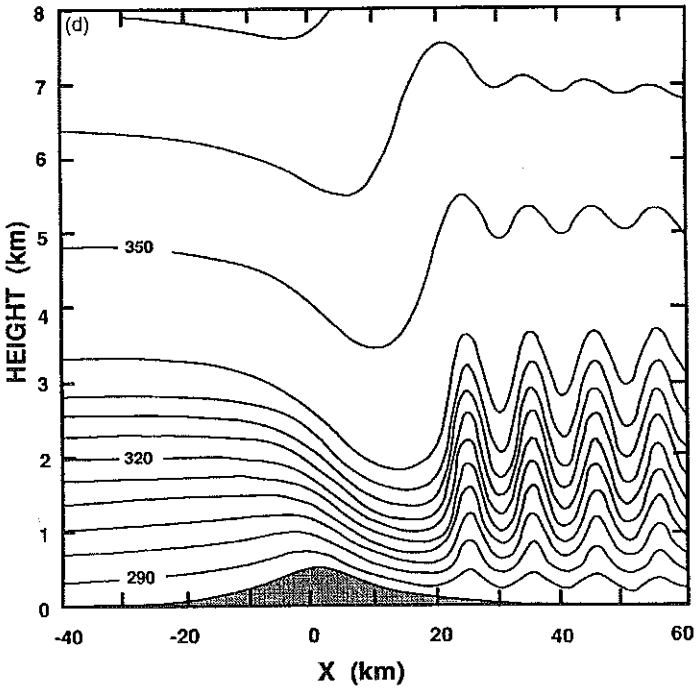

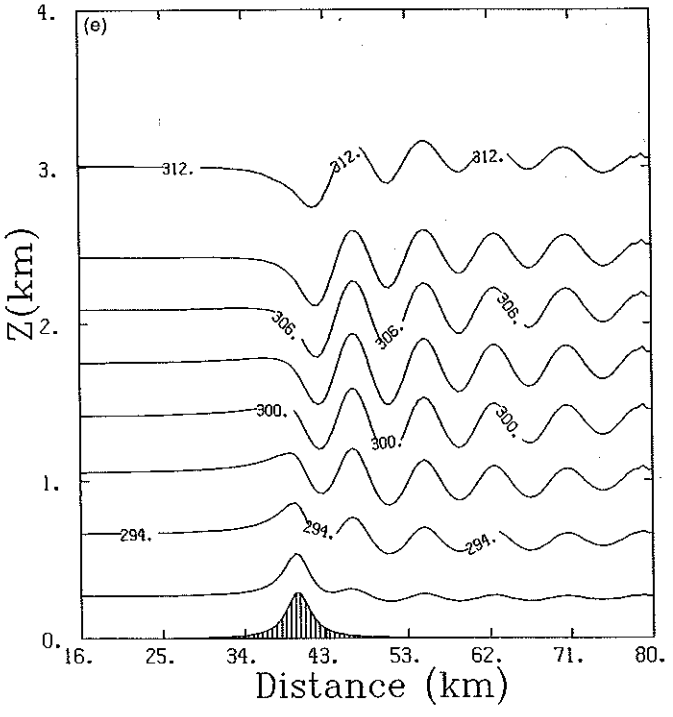

Figure 2. Continued.

3. Simulation of observed flows

Pitts and Lyons's (1989) observations for 13 December 1986 (Fig. 3(a)) and 3 February 1987 (Fig. 3(b)) were dominated by hydrostatic effects, whereas their 21 January 1987 observations (Fig. 3(c)) were nonhydrostatic with a train of resonant lee waves. The nonhydrostatic-model runs for the hydrostatically dominated days were initialized with the profiles used by Pitts and Lyons (1990), whereas for 21 January 1987 the data used are listed in Table 1. Figure 4(a) shows the development of the shooting flow and the downstream hydraulic jump for 3 February. It is similar to the simulations of Pitts and Lyons (1990) although the trough is slightly wider and there is an indication of a weak lee wave which decays rapidly downstream. To the lee of the escarpment wind speed increases to a maximum in the shooting flow and decreases behind the hydraulic jump (Fig. 4(b)). The model places a region of wind reversal beneath the crest of the lee wave, indicating the presence of a rotor, which is consistent with the observations (Fig. 3(b)).

Upstream and above the hydraulic jump the model indicates the presence of a calm region and the existence of a weak rotor. While it is not possible to verify this from the observations, it is interesting that the tank tests of Baines (1979) and Baines and Hoinka (1985) also suggest the presence of a weak rotor in this region.

Figure 4(c) illustrates the isentropic surfaces for 13 December 1986, which reproduce a very broad trough ending in a hydraulic jump, consistent with the observations (Fig. 3(a)) and previous simulations (Pitts and Lyons 1990). The model also indicates a weak train of lee waves beginning at the hydraulic jump, which the observations were unable to resolve. As the simulation reached steady state without propagation of the jump, it is correctly described as an undular jump. Rotors are found occurring under the crests of the lee waves, but these were not observed given the paucity of surface observations available.

The simulation for 21 January 1987 (Fig. 5(a)) shows a field of resonant lee waves with a crest-to-trough height of approximately 400 m and a wavelength of about 5 km. This is consistent with the observations (Fig. 3(c)). The cross-section of the modelled wind speeds (Fig. 5(b)) illustrates a wind decrease and reversal below the peaks of each lee wave.

The observations of 21 January 1987 also present a good opportunity for a comparison with the linear-model solution for a bell-shaped hill, as the flow was dominated by nonhydrostatic waves. The other advantage with this set of observations is that the critical layer was significantly higher than on other days. At the critical layer Scorer's parameter approaches infinity, invalidating the linear model, although the singularities arising can be treated using the technique of Frobenius (Simard and Peltier 1982). Furthermore, if Scorer's parameter aloft is anywhere greater than in the trapping region then lee-wave energy will leak away causing the waves to decay downstream (Smith 1979). Sawyer (1960) observed that while large variations in l^2 aloft significantly altered wave structure in the upper layers, there was a minimal effect on lee waves in the lower atmosphere.

To justify use of the profile below the critical level it is necessary to assume that trapping is confined below this region, and that the critical layer is high enough that it will not significantly affect wave propagation in the boundary layer. Therefore, only values of wind speed and temperature data below the critical layer were used. The resultant lee waves (Fig. 5(c)) have a maximum amplitude of 540 m and a wavelength of 8.3 km. The solution proved to be very sensitive to the assumption of trapping below the critical level and to how l^2 was prescribed in this region. This is compounded by the shallowness of the layer being studied. Previous lee-wave analysis by Mitchell *et al.*

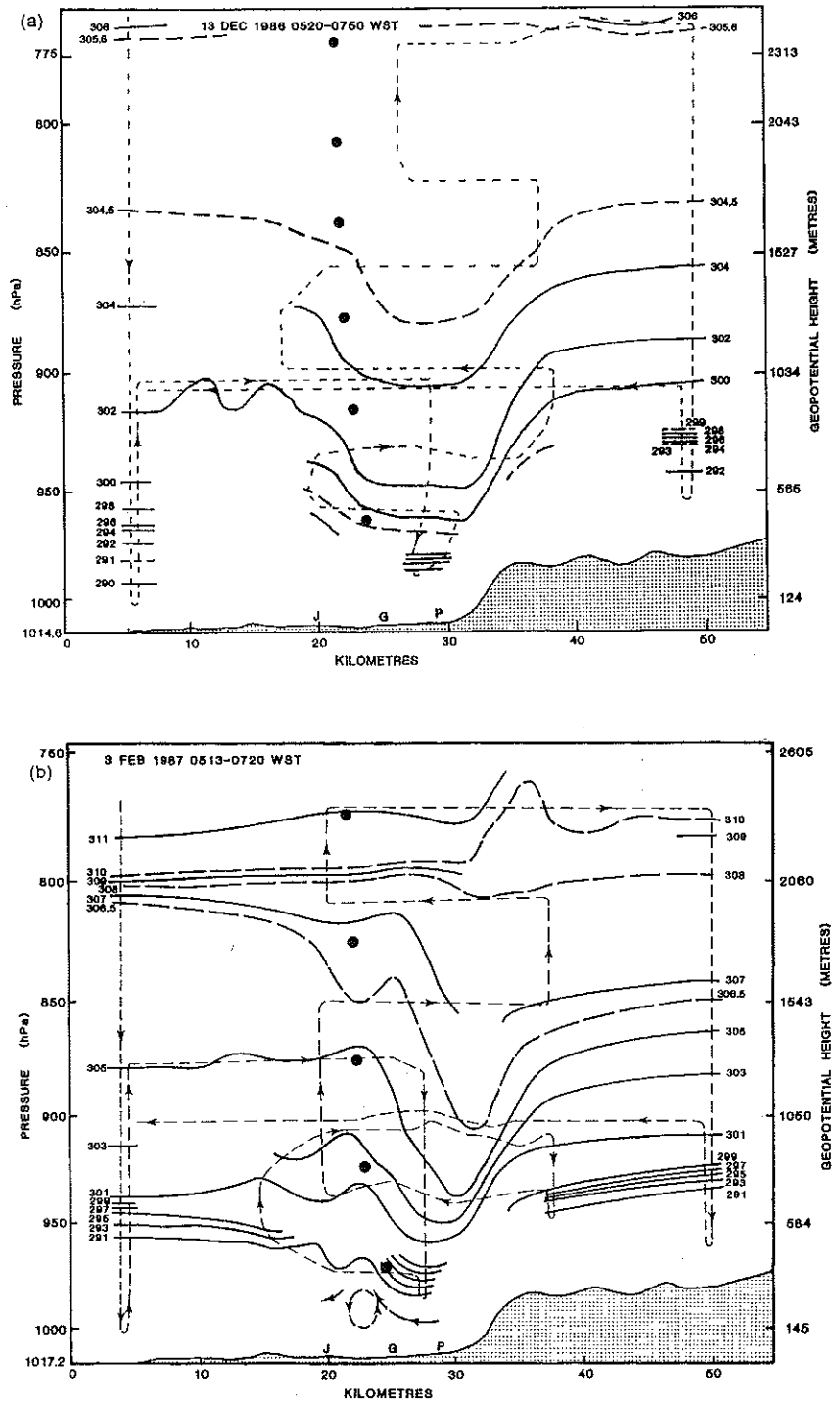

Figure 3. Isentropic surfaces observed on (a) 13 December 1986, (b) 3 February 1987 and (c) 21 January 1987. The large black dots indicate ascent paths of the radiosondes released from Perth airport (after Pitts and Lyons 1989).

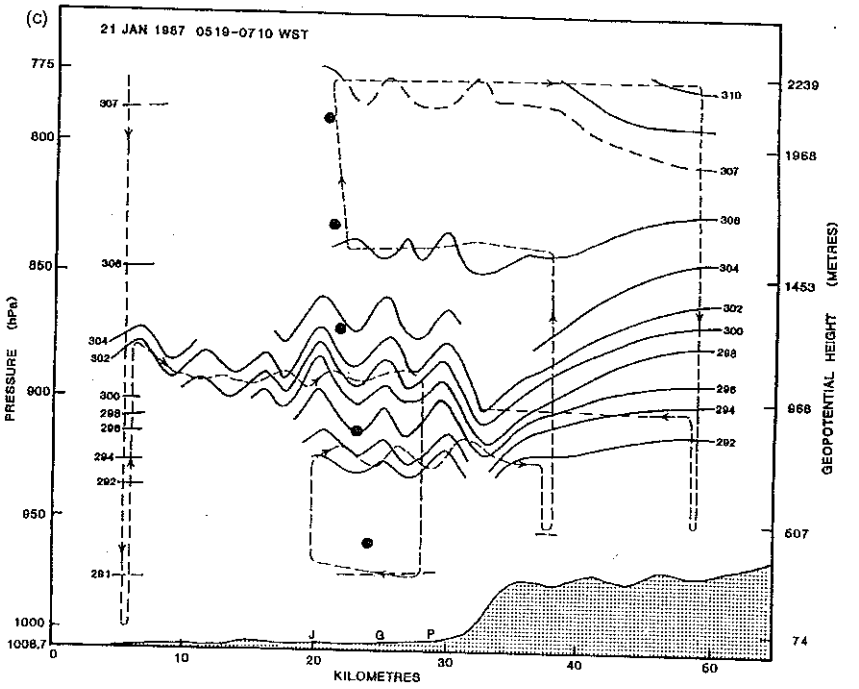

Figure 3. Continued.

TABLE 1. PROFILES OF WIND SPEED AND TEMPERATURE FOR 21 JANUARY 1987 USED TO INITIALIZE THE MODEL

Layer (m)	Shear (m^{-1})	Layer (m)	N (s^{-1})
0–335	−0.0053	0–440	0.0042
335–880	−0.0198	440–1440	0.02
880–2500	0.0161	1440–	0.0132
2500–3100	−0.0057		
3100–3900	0.000675		
3900–6100	0.0022		
6100–	0.0		

Surface wind speed = $-7.88\ m\ s^{-1}$.

(1990) of a ridge of similar height included a much deeper atmosphere of 10 km. The difficulty lies in that, while the critical layer is relatively high on this day, it is still very close to the wave-trapping layer. Clark and Peltier (1984), Bacmeister and Pierrehumbert (1988), Scinocca and Peltier (1991), and Smith (1979) have noted that the influence of critical layers on wave propagation or absorption dynamics is nonlinear and not well understood.

4. PRESSURE DRAG

As the wind speed over a mountain increases there is a pressure difference, and hence pressure drag, across the mountain. Pressure-drag histories provide a useful tool for observing the transition to the downslope windstorm configuration. Pressure drag is given by

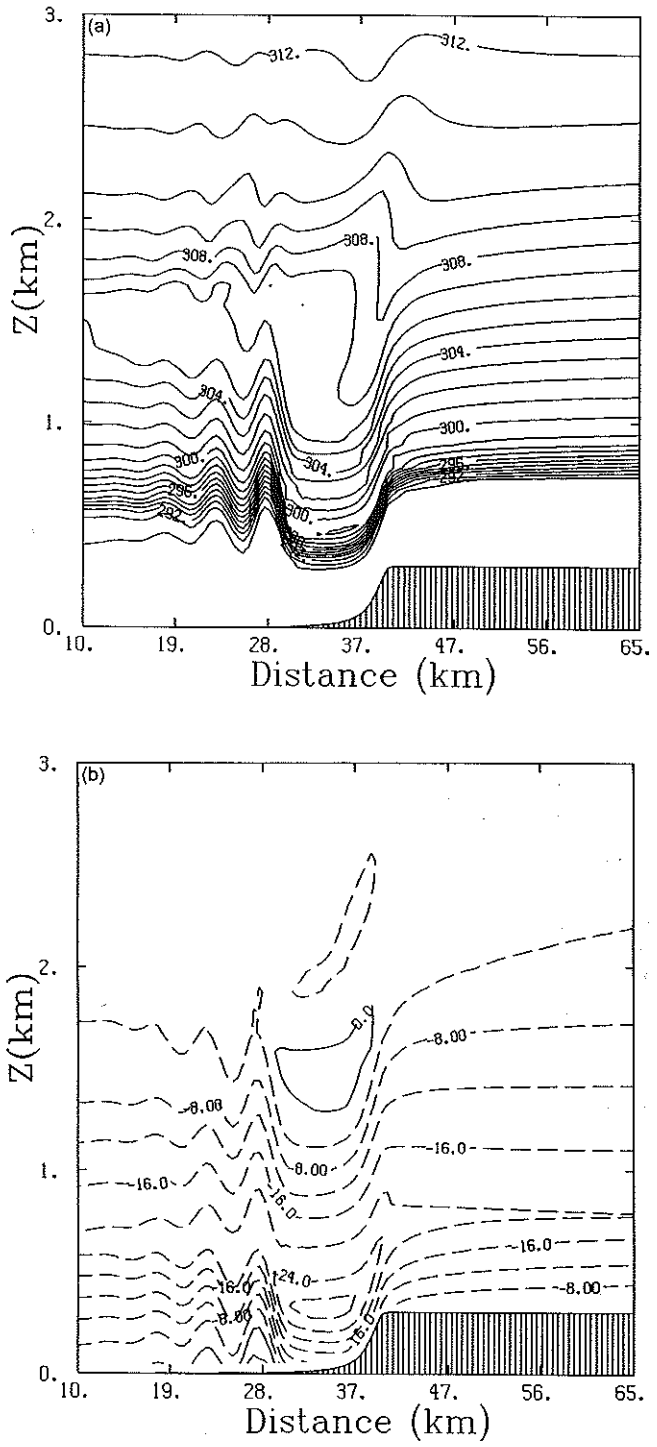

Figure 4. Model simulations of isentropic surfaces and U components of the flow for 3 February 1987 (a, b) and 13 December (c, d). Note that for comparison with the observations the flow is from right to left.

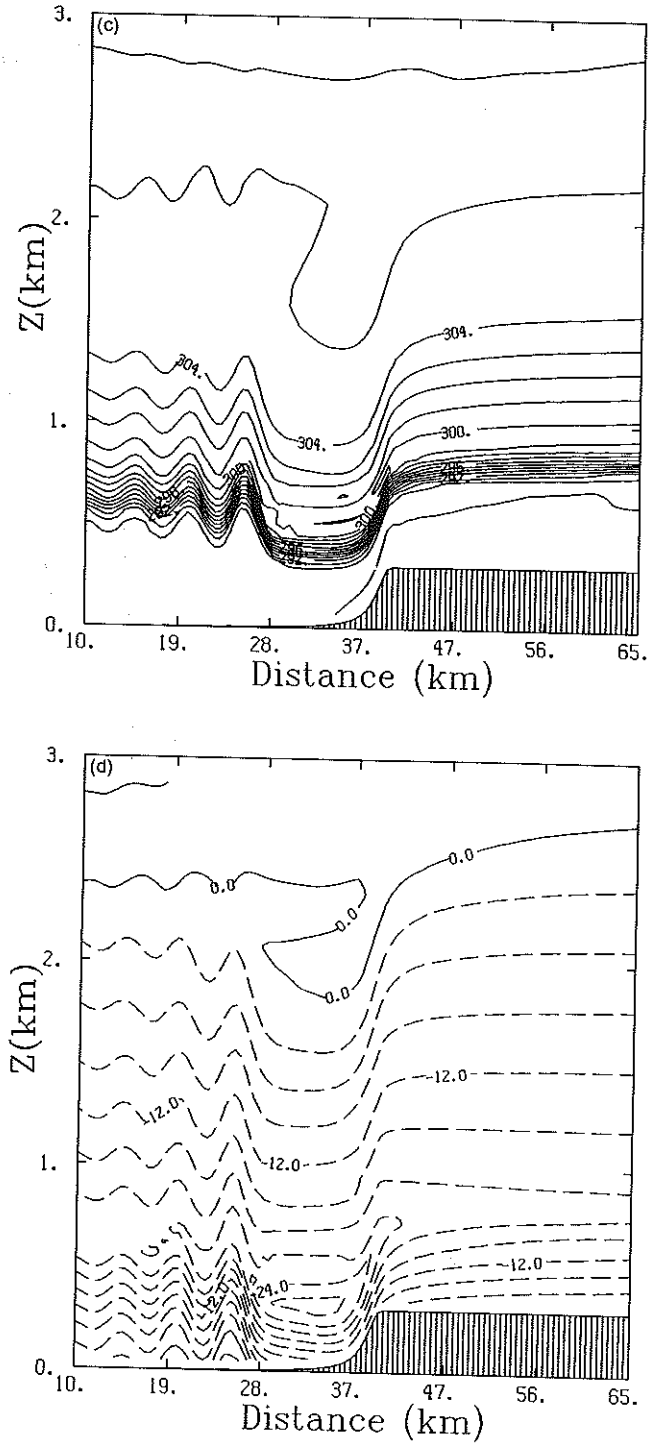

Figure 4. Continued.

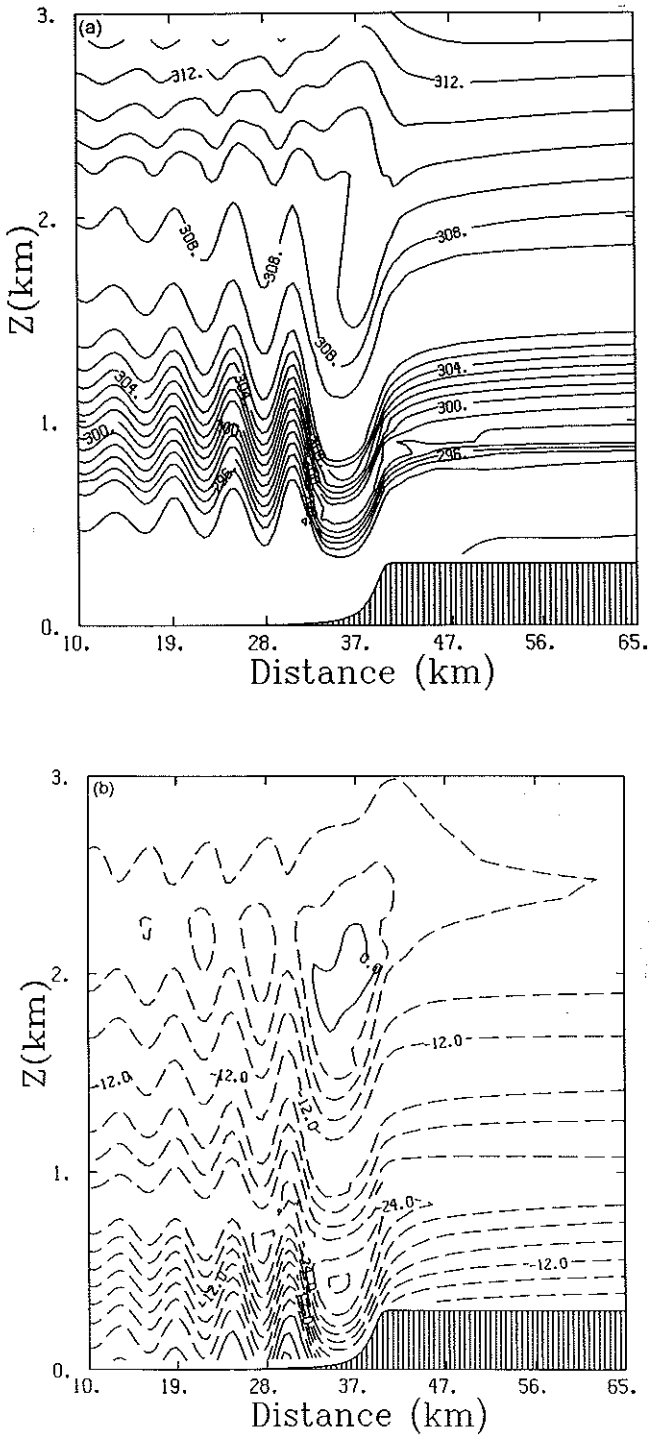

Figure 5. Model simulations of (a) isentropic surfaces, (b) U component of the flow for 21 January 1987 and (c) a linear-model result for a bell-shaped hill.

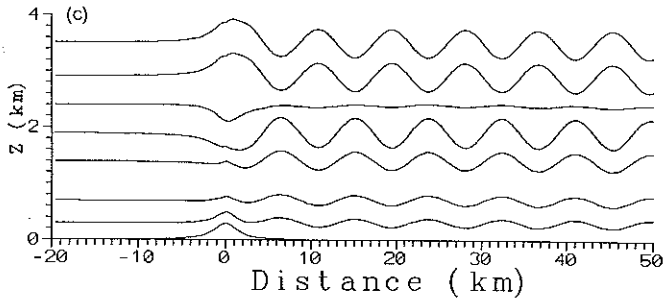

Figure 5. Continued.

$$D = \int_{-\infty}^{\infty} P' \frac{\partial h}{\partial x} \mathrm{d}x$$

where D is the surface pressure drag per metre, and P' is the pressure deviation from the hydrostatic reference pressure. Drag values are often normalized against the drag values predicted by linear theory for flows with constant wind speed and stability. For a bell-shaped hill this is given by $(\pi\rho NUh^2)/4$.

The numerical model's ability to predict drag was tested by obtaining the drag value from the numerical simulation of Klemp and Durran's (1983) analytical solution (Fig. 2(a)) and comparing it with the linear solution. The model-predicted value of $1.88 \times 10^4\,\mathrm{N\,m^{-1}}$ compared well with the value of $2.06 \times 10^4\,\mathrm{N\,m^{-1}}$ predicted by linear theory.

Previous studies have shown that drag increases if asymmetric topography is used. Ikawa (1990) calculated drag values for a range of asymmetric shapes, using linear and weakly nonlinear theory. For topography with gentle windward and steep leeward slopes there was a significant increase in drag for the nonlinear over the linear theory. Miles and Huppert (1969) in comparing drag for a number of topographic shapes noted that maximum wave steepening occurred at lower obstacle heights for the asymmetric topography. To determine whether the half-bell-shaped topography had any significant effect on drag the analytical simulation of Klemp and Durran (1983) was repeated using a half-bell-shaped escarpment. The final surface pressure drag of $1.28 \times 10^5\,\mathrm{N\,m^{-1}}$ is a significant increase over the value obtained by linear theory.

The simulations of 13 December 1986 and 3 February 1987 exhibit both nonhydrostatic and hydrostatic waves with a field of lee waves of varying strength developing behind the hydraulic jump. To better understand some of the processes behind these mixed solutions, and the possible effects of nonhydrostatic waves on windstorm events, a series of experiments (Table 2) were conducted that observed changes in drag history in response to changes in Na/U. In each experiment the mountain half-widths were varied such that Na/U covered a range of values between 1 and 10. Drag values have been normalized with respect to the linear drag for a bell-shaped hill for convenience, since it is not possible to calculate analytically the drag for asymmetric topography.

Figures 6 and 7 illustrate the evolution of drag for the single-layer experiments 1–4. For the bell-shaped hill the normalized drag remains about 1.0, reflecting the expected low drag state. By way of contrast, flow over the asymmetric topography results in a transition to a high drag state. It is also apparent that the transition to the high drag state becomes more pronounced as the flow becomes increasingly hydrostatic.

TABLE 2. PRESSURE-DRAG EXPERIMENT PARAMETERS

Experiment	Mountain shape	N (s^{-1})	U ($m\,s^{-1}$)	h (m)	a (m)
1	Bell	0.02	12.0	300	600
					1600
					3000
					6000
2	Half bell	0.02	12.0	300	600
					1600
					3000
					6000
3	Bell	0.02	12.0	450	600
					1600
					3000
					6000
4	Half bell	0.02	12.0	450	600
					1600
					3000
					6000
5	Bell	0.02 ($z \leq 3000$ m) 0.01 ($z > 3000$ m)	12.0	300	600
					1600
					3000
					6000
6	Half bell	0.02 ($z \leq 3000$ m) 0.01 ($z > 3000$ m)	12.0	300	600
					1600
					3000
					6000
7	Bell	0.02 ($z \leq 3000$ m) 0.01 ($z > 3000$ m)	24.0	600	600
					1600
					3000
					6000
8	Half bell	0.02 ($z \leq 3000$ m) 0.01 ($z > 3000$ m)	24.0	600	600
					1600
					3000
					6000

Increasing the mountain height to 450 m (Fig. 7) for the bell-shaped topography leads to a high drag response only for flows where $Na/U > 5$, whereas flows for the half-bell shape all evolve to a high drag state. These collapse after a non-dimensional time of 45, possibly from reflection off the lateral boundaries. It is also equally possible that the flows do not reach a steady state. Scinocca and Peltier (1991) tested the sensitivity of a range of flows to the Richardson number within the critical layer, and observed a number of cases in which the solutions did not appear to reach a steady state. There is also evidence (Scinocca and Peltier 1989) that oscillations within observed and modelled flows are a generic property of windstorms that are induced by the breaking of topographically forced waves.

Miles and Huppert (1969) suggest that wave breaking should occur for a bell-shaped hill when $Nh/U = 0.85$. Our value of 0.75 is a little lower than this; possibly the reflection off the model boundaries may have been sufficient to cause the gravity wave to break at the lower height.

The preceding single-layer experiments indicate that nonhydrostatic effects on flow that is dominated by the finite amplitude high drag state are a delay in the transition to the high drag state and a weaker final drag. They do not significantly modify the flow, which is in accord with the analysis of Bacmeister and Pierrehumbert (1988). These decreased responses are most likely a result of the reduced vertical transmission of the energy of nonhydrostatic flows.

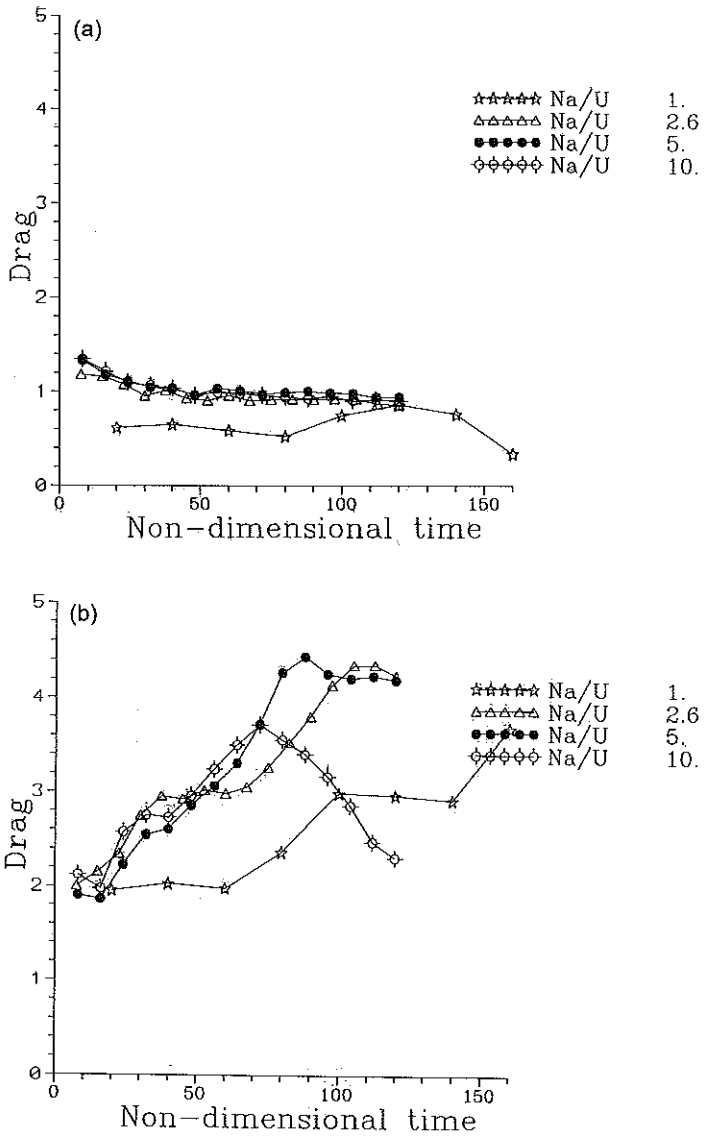

Figure 6. Pressure-drag evolution for experiments (a) 1 and (b) 2. See text and Table 2.

In order to observe the effect of trapped lee waves on the evolution of drag a further four experiments were carried out with a two-layer atmosphere. These experiments were carried out in a manner similar to experiments 1–4 (see Table 2) except that the Brunt–Väisälä frequency above 3000 m was reduced to 0.01 s^{-1}. Experiments 5 and 6 produced flows and drag responses (Fig. 8) very similar to experiments 1 and 2, except that for the bell-shaped hill, where there is no wave breaking, there is a much greater dependency of drag values on Na/U, suggesting increased partial reflection of waves off the interface between the two layers as Na/U increases. The resultant streamlines of experiments 5 and 6 (not shown) do not indicate any lee-wave modes in the solutions.

To see why this is so, it is necessary to compare the height of the interface between the two layers with the height of the breaking wave induced by mountain height and

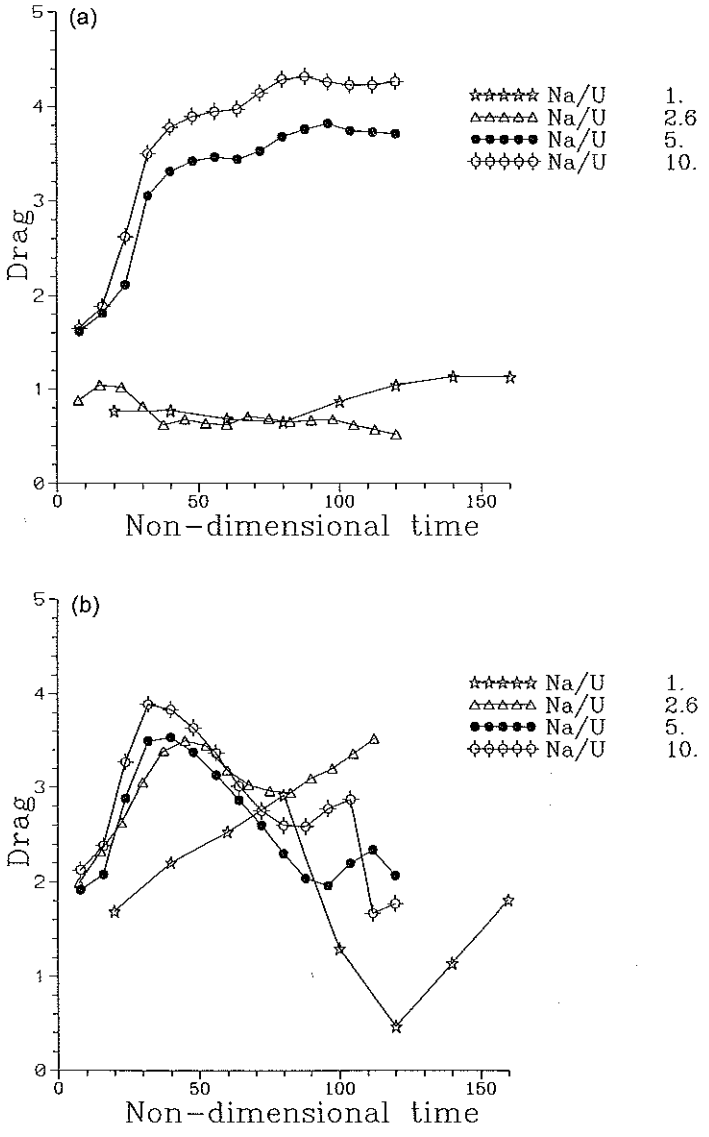

Figure 7. Pressure-drag evolution for experiments (a) 3 and (b) 4. See text and Table 2.

shape. For the purpose of the comparison the heights have been normalized with respect to the vertical wavelength ($\lambda_z = 2\pi U/N$). By assuming that the mean wind and stability vary little over a vertical wavelength Peltier and Clark (1979) have shown that wave breaking occurs at $3\pi/2$ for symmetric topography. In experiments 5 and 6 the layer interface lay at 1.6π, which is above the wave-breaking region. The experiments were repeated in 7 and 8 except that the normalized height of the layer interface was decreased to 0.8π by increasing the mountain height to 600 m. To ensure dynamic similarity with experiments 5 and 6 the wind speed was increased such that the same inverse Froude number was used in each experiment.

Although the streamlines for experiment 8 were similar to those of the hydrostatic days of 13 December and 3 February, in this case the shooting flow in the lee of the hill

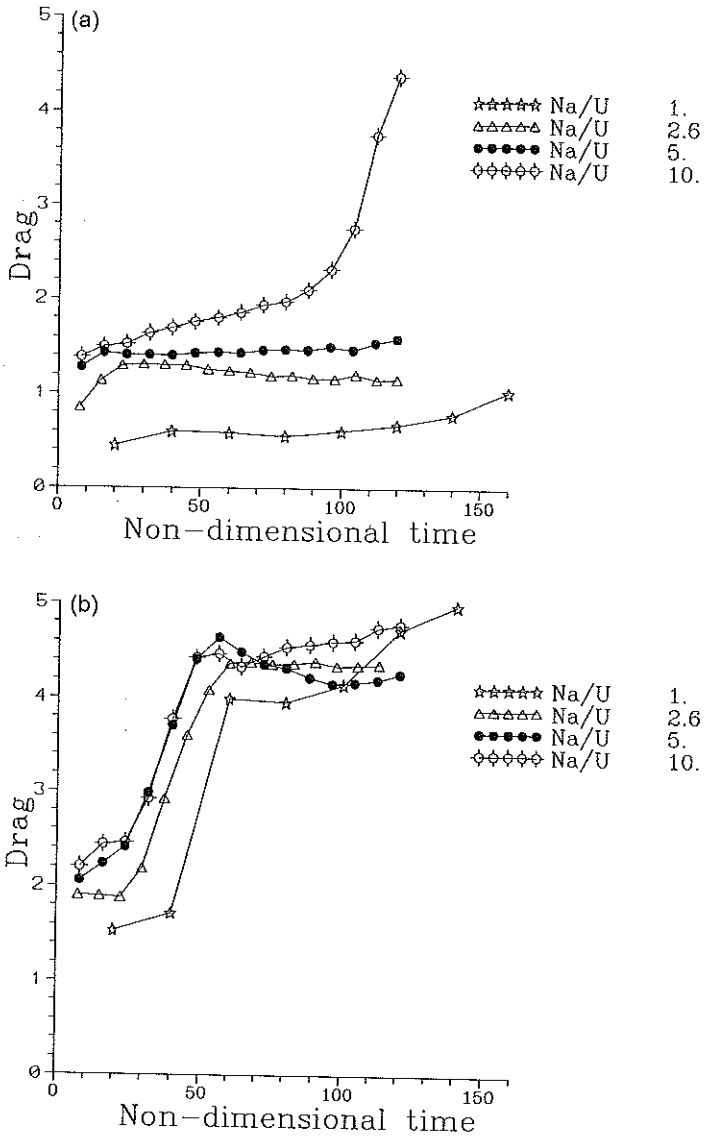

Figure 8. Pressure-drag evolution for experiments (a) 5 and (b) 6. See text and Table 2.

ended in a propagating undular bore. Like the lee waves examined earlier, the undular bore is essentially nonhydrostatic and cannot be captured by the hydrostatic model. It would appear that at least one condition for the undular bore is that trapping occurs below the wave-breaking region. The drag histories of experiment 8 (Fig. 9(b)) still show the same general features of previous simulations. The most significant difference being that after non-dimensional time 100 the drag begins to increase from the steady-state value. This time corresponds to the propagating jump reaching the downwind lateral boundary and is the result of numerical instabilities generated by reflection off that boundary.

In order to place the observed flows into the context of different flow types and the preceding drag experiments a regime diagram was constructed. Figure 10 shows the four

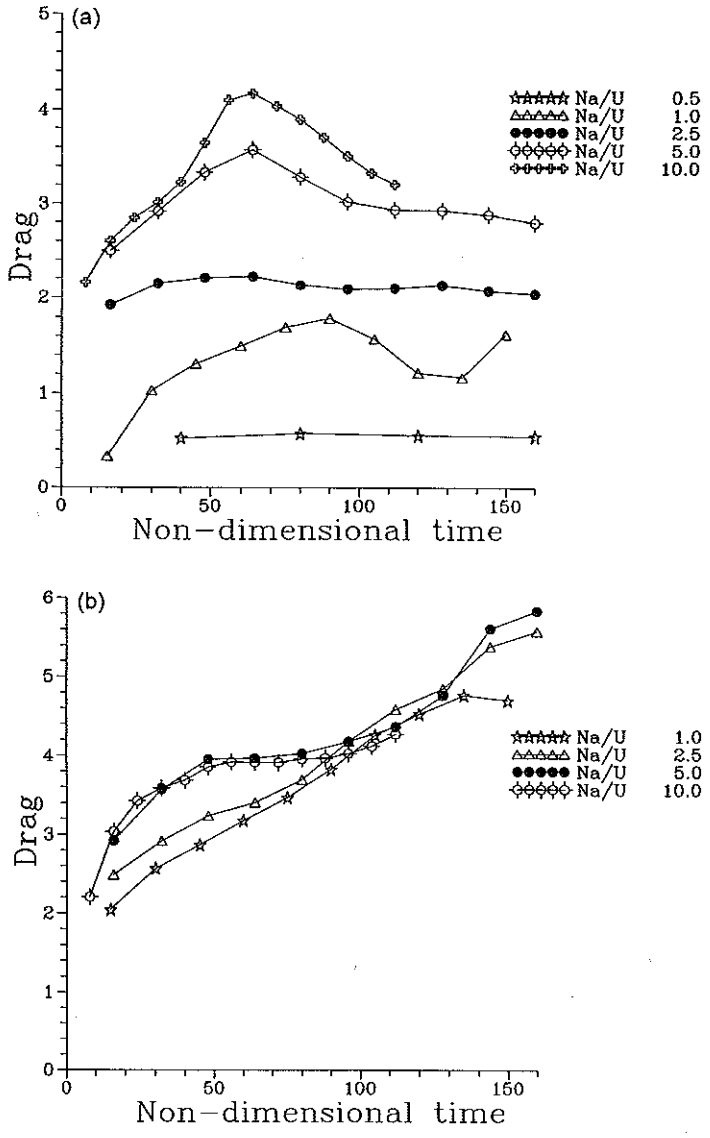

Figure 9. Pressure-drag evolution for experiments (a) 7 and (b) 8. See text and Table 2.

main flow regimes observed in the single- and double-layer simulations for flow over a half-bell-shaped ridge. Flow differentiation is based on the observation that no lee waves were found in the drag experiments for $U/Na < 0.3$ and onset of wave breaking occurred at $Nh/U \approx 0.5$. Flow type I represents vertically propagating gravity waves. As the non-dimensional mountain height increases, the wave steepens and eventually breaks, resulting in the high-drag regime of type II. Regime types III and IV represent two-layer flows in which lee waves are present in the solution. Type IV represents classical resonant lee waves and type III represents flows with a mixed-mode wave in the form of a stationary undular jump or propagating undular bore. It is worth noting that for type III flows the strongest mixed-mode solutions should exist for $U/Na \approx 0.3$. As U/Na

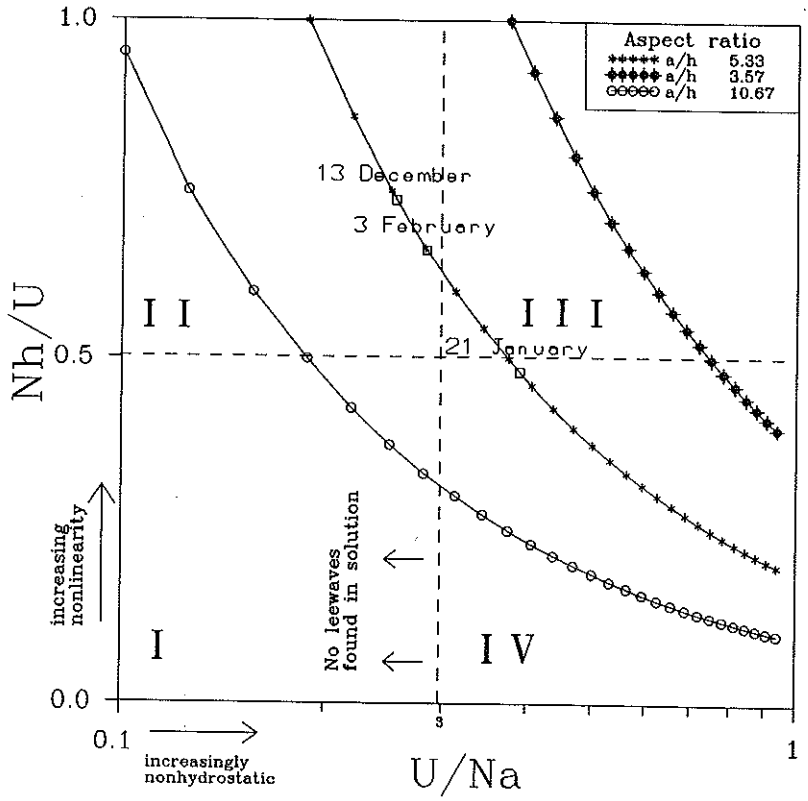

Figure 10. Regime diagram for nonsheared flow, with constant stability, over a half-bell-shaped escarpment. Different flow types are indicated as (I) vertically propagating gravity waves, (II) high-drag state induced by wave breaking, (III) mixed-mode waves with strong lee-slope winds and undular jumps or bores and (IV) flow dominated by trapped lee waves.

increases beyond this value, the waves become evanescent with reduced hydrostatic forcing of the lee-wave modes.

The three curves on Fig. 10 represent the solution fields for three different mountain shapes specified by an aspect ratio defined as a/h. This highlights the optimal shape and steepness of the Darling Scarp for the development of mixed-mode waves. If the ridge were too narrow (i.e. $a/h = 3.57$) the flow would be dominated by nonhydrostatic wavelengths and unlikely to develop strong hydrostatic forcing. Alternatively, a wider ridge would tend to show little evidence of lee waves.

A representative value of N/U for each of the days observed by Pitts and Lyons (1989) was obtained by using values in the lower layers, and these are shown on the solution curve for the Darling Scarp (Fig. 10). Although 3 February and 13 December are both strongly hydrostatically dominated days and can be categorized as flow type II, there was evidence in both the observations and numerical simulations of nonhydrostatic effects. These can be accounted for by noting the vertical variation in N/U. Thus while the regime diagram highlights the general flow type possible for a given upstream flow state, it does not account for vertical variations in wind speed or stability. This highlights the difficulty of defining a single N/U for such complex flows.

5. Sensitivity tests

The simulations for the hydrostatically dominated days, 13 December and 3 February, suggest nonhydrostatic effects were present. Pitts and Lyons (1990), using their hydrostatic model, were unable to examine the sensitivity of nonhydrostatic effects to changes in upstream forcing. In order to determine whether the nonhydrostatic waves evident on those days had any significant effect on their results, their experiments were repeated using the nonhydrostatic model. Only those simulations which produced significant differences from the original simulations are presented.

Figure 11 is based upon 3 February, except that the critical layer was removed by neglecting shear above 1600 m. In the nonhydrostatic simulation the breaking wave has a much larger amplitude and slightly narrower trough, indicating that some wave energy is able to leak vertically through the wave-breaking region. For the hydrostatic wave there is complete reflection of the vertically propagating wave irrespective of the presence of a critical layer. The most plausible explanation is that the strong vertical motion suggested by the simulation violates the hydrostatic assumption and, hence, is not adequately captured by the hydrostatic model.

Figure 12 shows the hydrostatic and nonhydrostatic solutions for the case where the observed wind for 3 February has been replaced by a constant wind field. In the hydrostatic case there is a vertically propagating gravity wave, in contrast the nonhydrostatic model shows a field of lee waves which decay with height. A position that is supported by an examination of the Scorer parameter, N/U, (Table 3) which is steadily decreasing with height above the boundary layer.

The inversion between 760 and 1500 m, observed on 13 December, was removed by setting N to 0.0164 s^{-1}. Figure 13 indicates that the shooting flow still develops to the lee of the escarpment but the hydraulic jump now occurs further downstream. Pitts and Lyons (1990) noted that by removing the inversion Na/U is reduced to 2.19, implying nonhydrostatic flow. However, there is little difference between the nonhydrostatic and hydrostatic fields, illustrating that the flow is predominantly hydrostatically forced.

In hydraulic theory the transition from subcritical to supercritical flow is determined by the inverse Froude number

$$Fr^{-1} = \frac{Nh}{U}$$

which characterizes the balance between the pressure-gradient force and nonlinear advection. By removing the inversion and hence reducing N, the flow must move further downstream before the pressure-gradient term can dominate and the flow return to subcritical through a hydraulic jump. This perhaps also explains the flow's sensitivity to roughness-length changes (Pitts and Lyons 1990). With an increased roughness length, and thus frictional drag, the flow decelerates faster and the jump moves upstream.

These would tend to suggest that the average hydrostatic index of 4.8 proposed by Pitts and Lyons (1989) is in itself not enough to differentiate between the flow types observed over the Darling Scarp. This is reinforced by the previous drag experiments which indicated high drag states evolving with Na/U as low as 1. On the modified profile for 13 December the influence of waves breaking as they approached the critical layer was significant enough to cause the evolution of the flow even though the hydrostatic index was not optimal.

The previous simulations studied the possibility of nonhydrostatic waves affecting flow that is essentially dominated by hydrostatic motion. The remaining simulations examine the converse modifying role of hydrostatic forcing of nonhydrostatic flow.

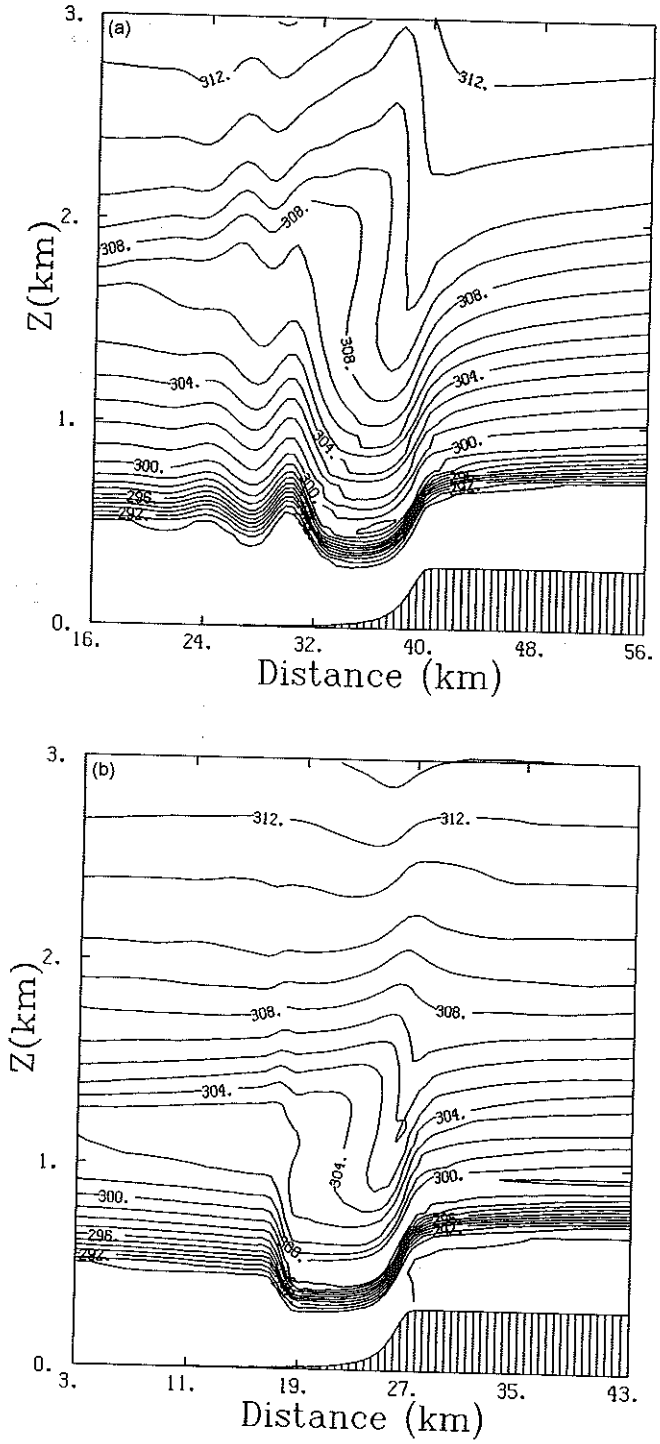

Figure 11. Predicted isentropic surfaces for 3 February assuming no critical level, (a) nonhydrostatic model and (b) hydrostatic model.

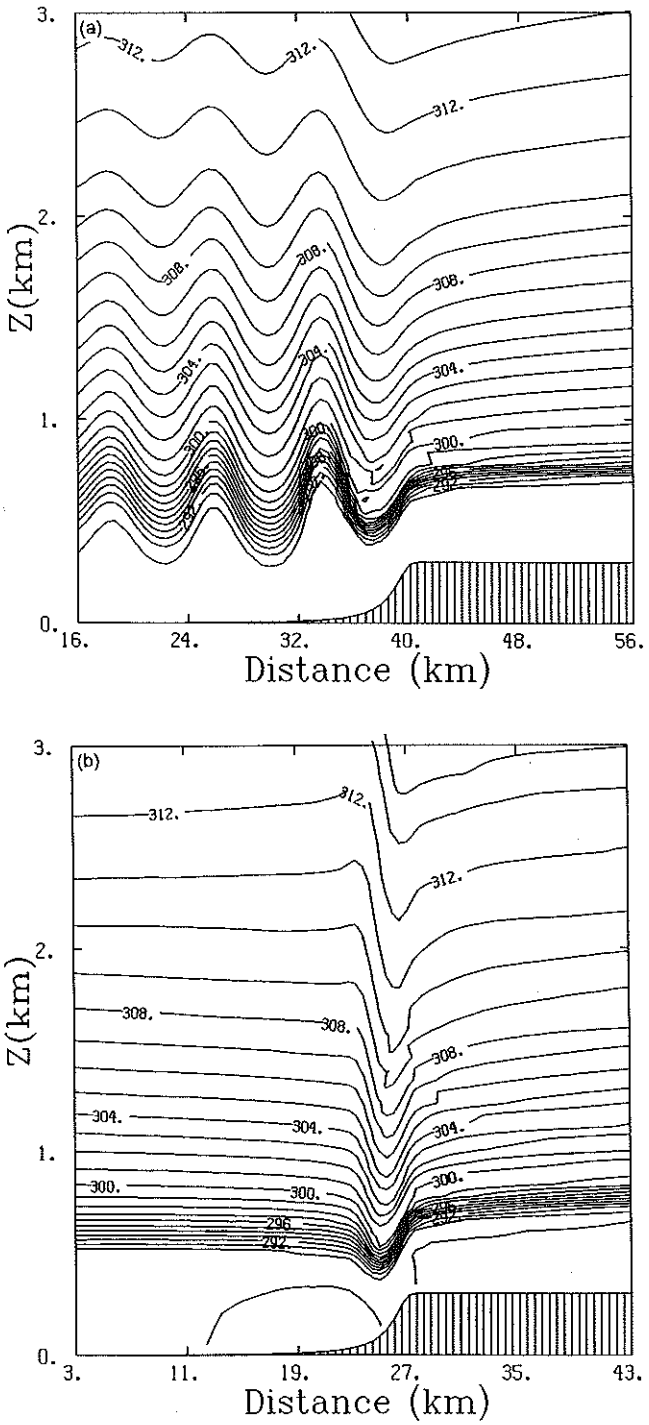

Figure 12. Predicted isentropic surfaces for 3 February assuming constant wind, (a) nonhydrostatic model and (b) hydrostatic model.

TABLE 3. ESTIMATED UPSTREAM VALUES FOR N/U, Nh/U AND Na/U OBTAINED FROM THE MODEL

Date	Layer (m)	N (s^{-1})	U ($m\,s^{-1}$)	N/U	Nh/U	Na/U
13 Dec.	0–560	0.008	8.4	0.00095	0.285	1.52
	560–740	0.045	18.3	0.0025	0.74	3.93
	740–1470	0.0173	13.4	0.00129	0.387	2.06
	1470–3270	0.0087	0	—	—	—
3 Feb.	0–440	0.0042	12.0	0.00035	0.105	0.56
	440–740	0.042	19.0	0.0022	0.66	3.54
	740–1970	0.02	9.6	0.0021	0.63	3.36
	1970–4700	0.012	1.3	0.0092		
3 Feb.	0–440	0.0042	11.5	0.00036	0.108	0.58
No critical layer	440–740	0.042	20.3	0.0021	0.66	3.52
	740–1970	0.02	12.9	0.0015	0.45	2.4
	1970–4700	0.012	1.5	0.008		
3 Feb.	0–440	0.0042	11.5	0.00036	0.11	0.58
Constant wind speed	440–740	0.042	20.3	0.0021	0.66	3.52
	740–1970	0.02	19.3	0.001	0.30	1.6
	1970–4700	0.012	17.1	0.0007	0.21	1.12
21 Jan.	0–500	0.007	11.5	0.00061	0.183	0.98
Strong shear	500–1220	0.03	18.7	0.0016	0.48	2.57
	1220–1670	0.0037	11.5	0.00039	0.117	0.62
	1670–2670	0.0136	6.2	0.0026	0.78	4.16
21 Jan.	0–500	0.007	12.6	0.00056	0.168	0.90
Weak shear	500–1220	0.03	21.0	0.0014	0.42	2.24
	1220–1670	0.037	18.3	0.00020	0.06	0.32
	1670–2670	0.0163	14.7	0.0011	0.33	1.76

U is the east–west velocity component, N is the Brunt–Väisälä frequency, a is the mountain half-width and h is the mountain height.

Observations of flow on 21 January contain the most strongly nonhydrostatic features. The wind profile for this day (Table 1) is characterized by a U-component maximum at 900 m followed by a region of strong shear where the wind speed rapidly drops to $-3.78\,m\,s^{-1}$ at 2500 m. Above this point the wind speed increases slightly before decreasing again. The critical level occurs at 5700 m, which is significantly higher than that observed for the hydrostatic days. As the critical layer is so high it is unlikely that it has a significant role to play in the development of waves in the boundary layer.

Richard *et al.* (1989) and Pitts and Lyons (1990) have shown that hydraulic flows are very sensitive to the frictional affects of the boundary layer. By repeating the 21 January simulation using a freeslip lower-boundary condition it was possible to show that there was hydrostatic forcing of the lee-wave structures observed on this day. In Fig. 14(a) the observed lee waves have been replaced by a propagating hydraulic jump.

Pitts and Lyons (1990) demonstrated that shear-induced wave breaking is a significant mechanism in the triggering of downslope windstorms. To examine the effect of the strong shear present in the layer between 900 and 2000 m the shear was reduced such that there was a constant wind shear between 900 m and the critical layer at 5700 m. The streamlines of the resultant simulation (Fig. 14(b)) are still dominated by lee waves which are somewhat weaker, though it is expected that these should also be directly influenced by changing the shear as this will affect the vertical profile of the Scorer parameter. Calculating the drag from the simulation of the observed flow ($8.05 \times 10^4\,N\,m^{-1}$) and comparing it with that of the weakened shear simulation ($3.79 \times 10^4\,N\,m^{-1}$) indicates a sufficient enough decrease in drag for the weakened shear case to suggest that the flow

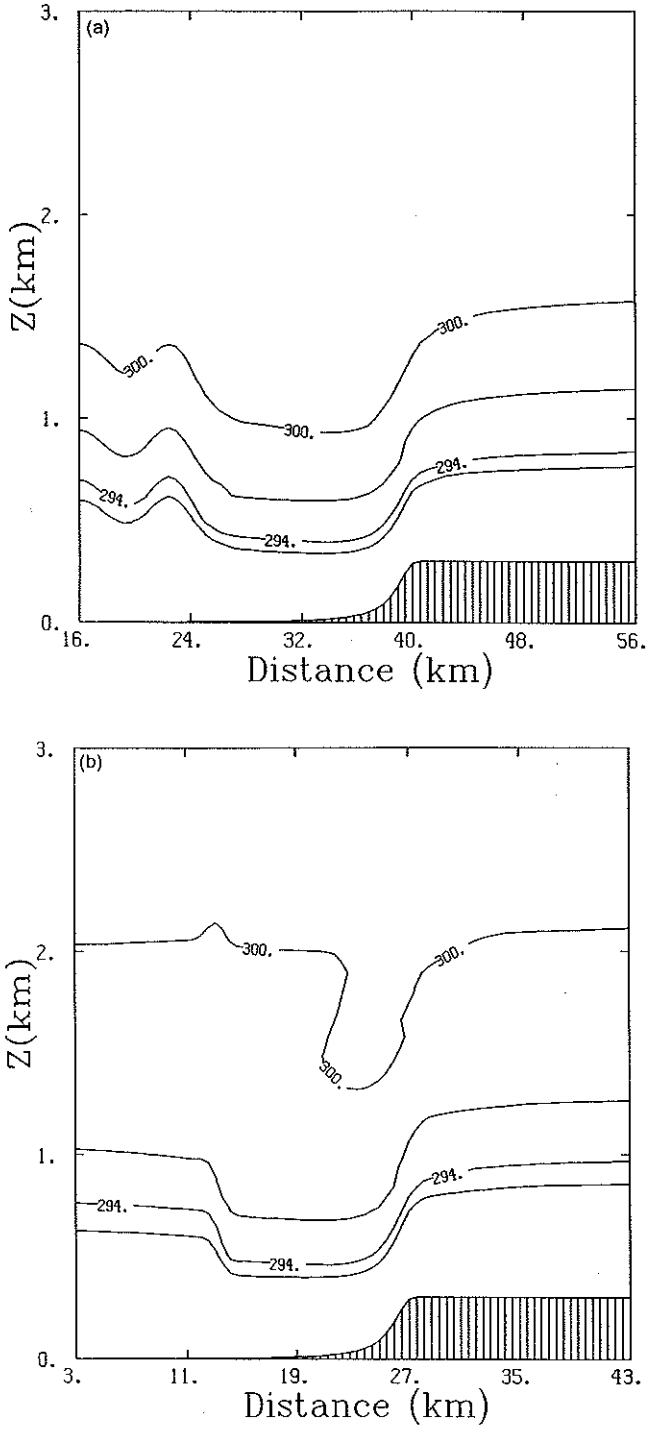

Figure 13. Predicted isentropic surfaces for 13 December assuming no inversion, (a) nonhydrostatic model and (b) hydrostatic model.

did not evolve into a high drag state. A more interesting comparison is obtained by repeating this simulation using a freeslip lower-boundary condition. In this case (Fig. 14(c)) there is no evidence of hydrostatic forcing and the flow remains dominated by trapped lee waves.

These simulations suggest a mixed-mode wave where both hydrostatic and non-hydrostatic waves exist in the flow and that there is significant hydrostatic forcing superimposed over the observed field of trapped lee waves. Hydrostatic forcing may affect the amplitude of the lee waves as shown in the comparison of linear theory with observations (Smith 1976). Furthermore, location of rotors and lee waves may also be sensitive to hydrostatic forcing. If rotors occur under crests of lee waves, and if the location of the hydraulic jump determines where lee waves begin, then it follows that the position of rotors may be sensitive to hydrostatic forcing. This is born out by our simulations that locate lee waves downwind of the hydraulic jump.

Numerical simulations by Saito and Ikawa (1991) also place the region of flow reversal to the leeward side of the hydraulic jump, although it is worth noting that the structure of the flow reversal obtained by them is somewhat different to ours. In their case the region of flow reversal can extend downstream for quite some distance and is not associated with lee waves. This can at least be partially explained by examining the parameter Na/U which took on approximate values between 20 and 60. These values are strongly hydrostatic, therefore it would not be expected for lee waves to develop. Saito and Ikawa (1991) also observed that the blocking effect of a second mountain range downstream of the hydraulic jump enhanced the strength of the flow reversal.

6. Conclusions

Previous differentiation of flow types observed to the lee of the Darling Scarp (Pitts and Lyons 1989) has been attempted using an average hydrostatic index. However, observation of drag histories, and sensitivity tests of observed flows indicate that it is possible for the flow to be dominated by hydrostatic downslope windstorms even if the hydrostatic index indicates nonhydrostatic dominance.

Experiments on a wide range of flows, consisting of one or two layers, with differing Na/U suggest that nonhydrostatic effects on windstorm events are very small. However, the development and location of trapped lee waves can be significantly affected if there is sufficient hydrostatic forcing in the flow. For hydrostatic forcing to dominate over trapped lee waves it is necessary for reflection, from a region of wave breaking or a critical layer, to occur at the right height. Miles and Huppert (1969) suggest a value of 0.58 for the inverse Froude number that will support wave breaking in nonsheared flow over topography with shallow windward slope and steep leeward slope. Numerical simulations of nonsheared flows (e.g. experiment 2, Table 2) had wave breaking for values of Nh/U as low as 0.50 for the half-bell-shaped escarpment. While reflection from the lateral boundaries may result in this latter figure being too low it would not be unreasonable to suggest that a plausible value for wave breaking over the Darling Scarp should lie somewhere between these two values.

Construction of a regime diagram incorporating the effects of ridge height and width suggest that the Darling Scarp has an optimal aspect ratio for the development of mixed-mode waves under simple two-layer flows. With more complex flows, lee wave development is sensitive to variations in l^2 aloft.

An analysis of the nonhydrostatically dominated day using a linear lee-wave model indicated that the flow is very sensitive to specification of l^2 below the critical layer. Critical-layer dynamics are nonlinear, and complex flows such as those observed over

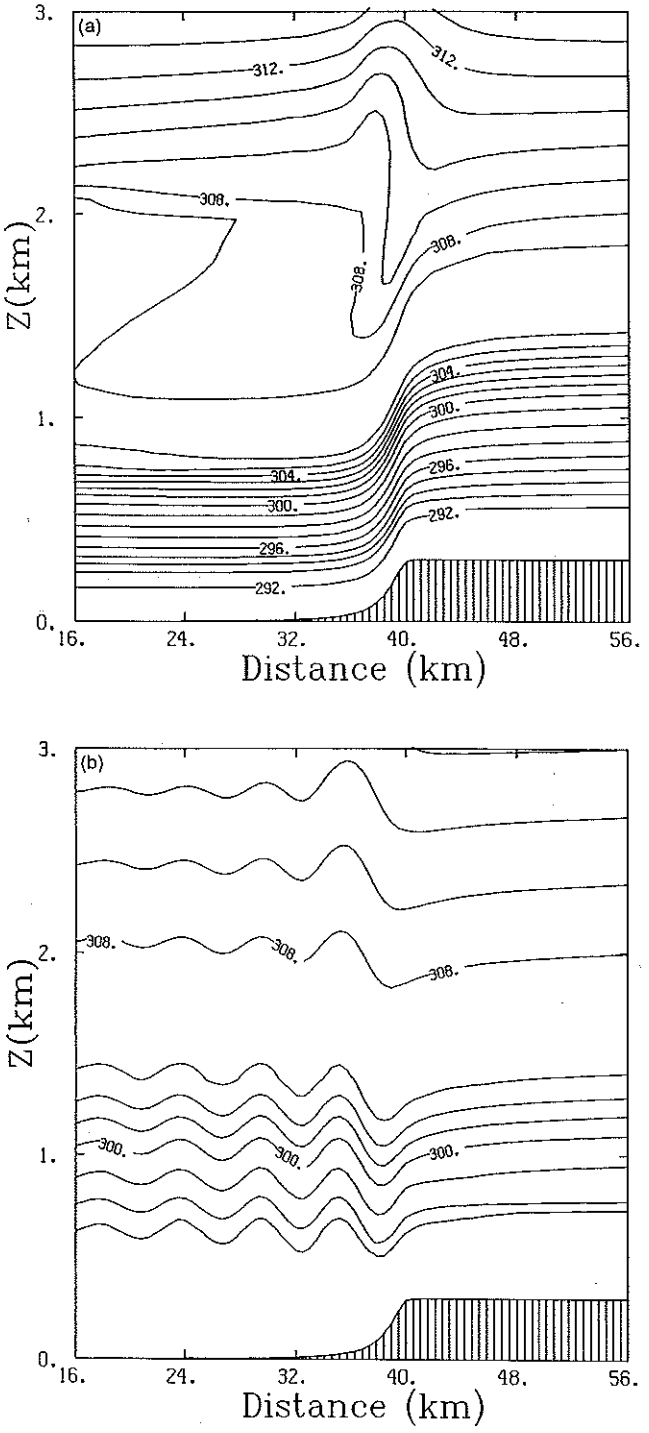

Figure 14. Predicted isentropic surfaces for 21 January assuming (a) freeslip boundary, (b) weak shear, and (c) weak shear and a freeslip boundary.

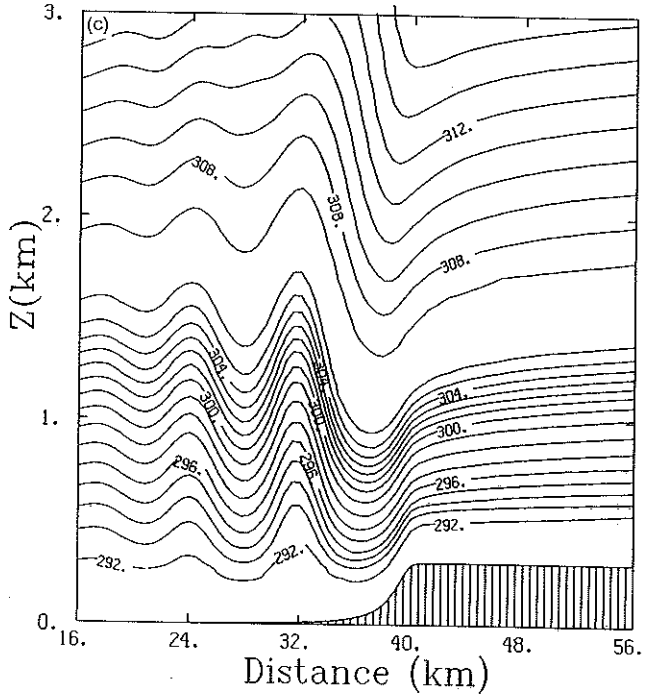

Figure 14. Continued.

the Darling Scarp do not lend themselves well to purely linear analysis. Nevertheless, the modifying role of the critical layer on the structure of lee waves is not well understood and will be the subject of future analysis.

Acknowledgements

This research was supported by the Australian Research Council. The RAMS code was provided by Professor Roger Pielke, and RAMS was developed under the support of the National Science Foundation (NSW) and the Army Research Office. Comments by an anonymous referee have enhanced the paper. All of this assistance is gratefully acknowledged.

References

Asselin, R. 1972 Frequency filter for time integrations. *Mon. Weather Rev.*, **100,** 487–490

Bacmeister, J. T. and Pierrehumbert, R. T. 1988 On high-drag states of non-linear stratified flow over an obstacle. *J. Atmos. Sci.*, **45,** 63–80

Baines, P. G. 1979 Observations of stratified flow over two-dimensional obstacles in fluid of finite depth. *Tellus*, **31,** 351–371

Baines, P. G. and Hoinka, K. P. 1985 Stratified flow over two-dimensional topography in fluid of infinite depth: a laboratory simulation. *J. Atmos. Sci.*, **42,** 1614–1630

Clark, T. L. and Peltier, W. R. 1984 Critical level reflection and the resonant growth of nonlinear mountain waves. *J. Atmos. Sci.*, **41,** 3122–3133

Cotton, W. R. and Tripoli, J. 1978 Cumulus convection in shear flow—three-dimensional numerical experiments. *J. Atmos. Sci.*, **35,** 1503–1521

Davies, H. C.	1983	Limitations of some common lateral boundary schemes used in regional NWP models. *Mon. Weather Rev.*, **111,** 1002–1012
Durran, D. R.	1986	Another look at downslope windstorms. Part I: The development of analogues to supercritical flow in an infinitely deep continuously stratified fluid. *J. Atmos. Sci.*, **43,** 2527–2543
Durran, D. R. and Klemp, J. B.	1987	Another look at downslope windstorms. Part II: Nonlinear amplification beneath wave overturning layers. *J. Atmos. Sci.*, **44,** 3402–3412
Ikawa, M.	1990	Weakly non-linear aspects of steady hydrostatic mountain waves in a 2-layered stratified fluid of infinite depth over a 2-dimensional mountain. *J. Meteorol. Soc. Japan*, **68,** 357–369
Klemp, J. B. and Durran, D. R.	1983	An upper boundary condition permitting internal gravity wave radiation in numerical mesoscale models. *Mon. Weather Rev.*, **111,** 430–444
Klemp, J. B. and Lilly, D. K.	1980	Mountain waves and momentum flux. Pp. 116–141 in *Orographic effects in planetary flows.* GARP series No. 23, World Meteorological Organization
Laprise, R. and Peltier, W. R.	1989	The linear stability of nonlinear mountain waves: implications for the understanding of severe downslope windstorms. *J. Atmos. Sci.*, **45,** 545–564
McNider, R. T. and Pielke R. A.	1984	Numerical simulation of slope and mountain flows. *J. Climate Appl. Meteorol.*, **23,** 1441–1453
Miles, J. W. and Huppert, H. E.	1969	Lee waves in a stratified flow. Part 4. Perturbation approximation. *J. Fluid Mech.*, **35,** 497–525
Mitchell, R. M., Cechet, R. P., Turner, P. J. and Elsum, C. C.	1990	Observation and interpretation of wave clouds over Macquarie Island. *Q. J. R. Meteorol. Soc.*, **116,** 741–752.
Orlanski, I.	1976	A simple boundary condition for unbounded hyperbolic flows. *J. Comput. Phys.*, **21,** 251–269
Peltier, W. R. and Clark, T. L	1979	The evolution and stability of finite amplitude mountain waves. Part 2: Surface wave drag and severe downslope windstorms. *J. Atmos. Sci.*, **36,** 1498–1529
	1983	Nonlinear mountain waves in two and three spatial dimensions. *Q. J. R. Meteorol. Soc.*, **109,** 527–548
Pitts, R. O. and Lyons, T. J.	1989	Airflow over a two-dimensional escarpment. I: Observations. *Q. J. R. Meteorol. Soc.*, **115,** 965–981
	1990	Airflow over a two-dimensional escarpment. II: Hydrostatic flow. *Q. J. R. Meteorol. Soc.*, **116,** 363–378
Richard, E., Mascart, P., Nickerson, E. C.	1989	The role of surface friction in downslope windstorms. *J. Appl. Meteorol.*, **28,** 241–245
Saito, K. and Ikawa, M.	1991	A numerical study of the local downslope wind 'Yamajikaze' in Japan. *J. Meteorol. Soc. Japan.*, **69,** 31–56
Sawyer, J.	1960	Numerical calculation of the displacements of a stratified airstream crossing a ridge of small height. *Q. J. R. Meteorol. Soc.*, **86,** 326–345
Scinocca, J. F. and Peltier, W. R.	1989	Pulsating downslope windstorms. *J. Atmos. Sci.*, **46,** 2885–2914
	1991	On the Richardson number dependence of nonlinear critical-layer flow over localised topography. *J. Atmos. Sci.*, **48,** 1560–1572
Scorer, R. S.	1949	Theory of waves in the lee of mountains. *Q. J. R. Meteorol. Soc.*, **75,** 41–56
Simard, A. and Peltier, W. R.	1982	Ship waves in the lee of isolated topography. *J. Atmos. Sci.*, **39,** 587–609
Smith, R. B.	1976	The generation of lee waves by the Blue Ridge. *J. Atmos. Sci.*, **33,** 507–519
	1979	The influence of mountains on the atmosphere. *Adv. Geophys.*, **21,** 87–230
	1985	On severe downslope winds. *J. Atmos. Sci.*, **42,** 2597–2603
Tremback, C. J., Powell, J., Cotton, W. R. and Pielke R. A.	1985	The forward-in-time upstream advection scheme: Extension to higher orders. *Mon. Weather Rev.*, **115,** 540–555

Tripoli, G. J. and Cotton, W. R. 1982 The Colorado State University three-dimensional cloud/mesoscale model—1982. Part I: General theoretical framework and sensitivity experiments. *J. Rech. Atmos.*, **16,** 185–219

Vergeiner, I. 1971 An operational linear lee wave model for arbitrary basic flow and two-dimensional topography. *Q. J. R. Meteorol. Soc.*, **97,** 30–60